Quantum and classical studies of vibrational motion of CH_5^+ on a global potential energy surface obtained from a novel *ab initio* direct dynamics approach

Alex Brown[a)]
Department of Chemistry and Cherry L. Emerson Center for Scientific Computation, Emory University, Atlanta, Georgia 30322

Anne B. McCoy[b)]
Department of Chemistry, The Ohio State University, Columbus, Ohio 43210

Bastiaan J. Braams,[c)] Zhong Jin, and Joel M. Bowman[d)]
Department of Chemistry and Cherry L. Emerson Center for Scientific Computation, Emory University, Atlanta, Georgia 30322

(Received 28 April 2004; accepted 2 June 2004)

We report a full dimensional, *ab initio* based potential energy surface for CH_5^+. The *ab initio* electronic energies and gradients are obtained in direct-dynamics calculations using second-order Møller-Plesset perturbation theory with the correlation consistent polarized valence triple zeta basis. The potential energy and the dipole moment surfaces are fit using novel procedures that ensure the full permutational symmetry of the system. The fitted potential energy surface is tested by comparing it against additional electronic energy calculations and by comparing normal mode frequencies at the three lowest-lying stationary points obtained from the fit against *ab initio* ones. Well-converged diffusion Monte Carlo zero-point energies, rotational constants, and projections along the CH and HH bond lengths and the tunneling coordinates are presented and compared with the corresponding harmonic oscillator and standard classical molecular dynamics ones. The delocalization of the wave function is analyzed through comparison of the CH_5^+ distributions with those obtained when all of the hydrogen atoms are replaced by ^2H and ^3H. The classical dipole correlation function is examined as a function of the total energy. This provides a further probe of the delocalization of CH_5^+. [DOI: 10.1063/1.1775767]

I. INTRODUCTION

The structure and dynamics of CH_5^+ have been problems of long-standing interest due to the extremely small (relative to the harmonic zero-point energy) barriers to internal rearrangement of the hydrogen atoms and its unusual bonding—three-center two-electron and four-center four-electron. Numerous quantum chemical studies[1–9] have been performed to characterize the relative energetics, and, in some cases, the normal modes, of the low-lying stationary points on the potential energy surface. These studies have focused on the relative energetics of the C_s(I), C_s(II), and C_{2v} stationary points on the potential, as depicted in Fig. 1. The general conclusion is that while the C_s(I) structure is the global minimum, once zero-point energy is taken into account (in the harmonic approximation), there may be no barrier to complete hydrogen scrambling. Indeed, the fluxional nature of CH_5^+ has also been borne out in Car-Parrinello dynamics simulations.[10–12] However, recent quasiclassical simulations of vibrational motions of CH_5^+ have suggested that some motions may be localized.[13]

While there have been numerous theoretical studies of the CH_5^+ ion, spectroscopic signature eluded experimentalists for many years. It is only recently that Oka and co-workers[14] were able to measure the infrared rovibrational spectrum of CH_5^+; the spectrum contains 900 lines in the region 2770–3150 cm^{-1}. However, the spectrum remains completely unassigned except for the qualitative assignment of lines in this region to C-H stretches; the CH_5^+ ion is produced rotationally hot which adds to the spectral congestion. The eventual goal of the present work is to use classical, semiclassical, and eventually quantum dynamics to help to assign the spectrum of CH_5^+. Previously, Tse, Klug, and Laasonen[3] reported the vibrational density of states for CH_5^+ evaluated from the Fourier transform of the velocity autocorrelation function in a Car-Parrinello molecular dynamics simulation. However, the experimental spectrum had not been reported at that time so no detailed comparison was made. Also, density functional theory, upon which the Car-Parrinello method is based, does not correctly reproduce the relative energetics of the low-lying isomers of CH_5^+,[7] and thus, while Car-Parrinello dynamics may give a good qualitative picture of the dynamics of CH_5^+ vibrational motion, its

[a)]Permanent Address: Department of Chemistry, University of Alberta, Edmonton, AB, T6G 2G2, Canada.
[b)]Electronic mail: mccoy@chemistry.ohio-state.edu
[c)]Also at Department of Mathematics and Computer Science, Emory University, Atlanta, GA 30322.
[d)]Electronic mail: bowman@euch4e.chem.emory.edu

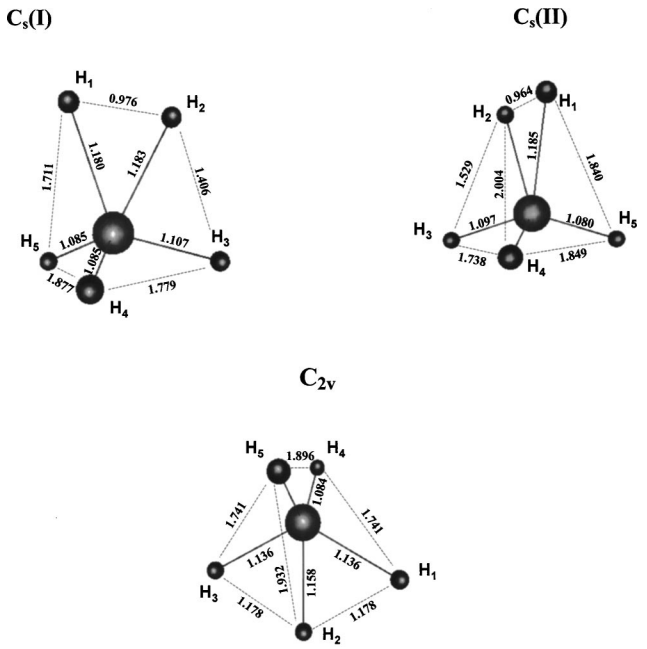

FIG. 1. Illustrations of the minimum energy C_s(I) conformer of CH_5^+, the low-lying C_s(II) transition state, and the low-lying C_{2v} transition state.

use for detailed quantitative studies, e.g., a vibrational spectrum, is questionable.

In order to investigate the dynamics (quantum, semiclassical, or classical), of CH_5^+ in detail and over long time scales or large regions of configuration space, a potential energy surface (PES) is needed. In two recent papers,[13,15] we reported a semiglobal PES for CH_5^+ that was used for low-energy classical trajectories[13] and a second PES utilizing additional *ab initio* data to extend the range of the PES to higher energies.[15] It was necessary to extend the range of points so that the fit is accurate over the range of the potential that is expected to be sampled by low-lying vibrational states of the ion. In the more recent paper, results of a preliminary analysis of the zero-point structure of CH_5^+ were discussed. Both potential surfaces were based on fitting electronic energies and gradients obtained by classical ''direct dynamics.'' In this paper, we describe the approach we have used to generate the potential surface in detail. We also present more extensive analysis and discussion of diffusion Monte Carlo (DMC) and molecular dynamics calculations done on this newer surface.

In the following section we describe the details of the calculation of electronic energies of CH_5^+ and the fitting of those data. Following that we present several tests of the PES that demonstrate the precision of the fit. The details of the DMC and classical molecular dynamics calculations are then presented. Results and discussion are given in Sec. III and we summarize and state our conclusions in Sec. IV.

II. METHODS AND CALCULATIONAL DETAILS

A. *Ab initio* molecular dynamics

In this section, we review the aspects of *ab initio* classical molecular dynamics (AIMD) calculations relevant to the present work. The classical Hamiltonian in Cartesian coordinates is given by

$$H=\sum_i \frac{P_i^2}{2m_i}+V(\mathbf{Q}), \tag{1}$$

where $\mathbf{Q}(t)$ represents all nuclear coordinates of the atoms, $\mathbf{P}(t)$ represents the corresponding momenta, and $V(\mathbf{Q})$ is the potential energy. While a variety of methods exist for integrating Hamilton's equations of motion, the most important piece of information that is required is the gradient of the potential. In AIMD, rather than having a global fit to the potential from which the gradient can be determined, the gradient is computed as needed along the trajectory, i.e., at each time step during the propagation.

For our purpose we choose to run trajectories with fixed total (potential+kinetic) energy. The initial geometry, $\mathbf{Q}(t=0)$, is taken to be that at the global minimum of the potential, which is of C_s symmetry and is denoted C_s(I). Therefore, the initial potential energy is zero. Initially the atoms are given random velocities, after which the center-of-mass motion is removed, the total angular momentum is set to zero, and the velocities are uniformly rescaled to give the desired initial total energy, which is all in the form of kinetic energy.

Trajectories were numerically integrated using the velocity-Verlet algorithm.[16] Depending on the initial total energy, time steps of 5, 10, or 40 a.u. (approximately 0.1, 0.2, or 1.0 fs) were utilized. The total energy was conserved to within 5 cm^{-1}, for all AIMD trajectories. In addition, these time steps also provided excellent conservation of linear and angular momenta, i.e., they remained (nearly) zero.

The potential energies and gradients were determined using second-order Møller-Plesset perturbation theory [(MP2) Ref. 17] with the correlation consistent polarization valence triple zeta (cc-pVTZ) basis set of Dunning;[18] calculations that shall be denoted cc-pVTZ/MP2. For the hydrogen atoms and carbon atom, the $(5s,2p,1d)/[3s,2p,1d]$ and $(10s,5p,2d,1f)/[4s,3p,2d,1f]$ contractions were used, respectively. Only the valence electrons were included in the correlation part of the calculation. The MP2 method was chosen due to its accuracy, efficiency, and the availability of analytical gradients.[19] All electronic structure calculations were carried out using the MOLPRO suite of electronic structure codes.[20] This level of *ab initio* calculation will allow us to demonstrate the utility of using direct dynamics data (potential energies and gradients) to obtain a potential energy surface and will allow quantitative study of the dynamics and ground state wave function of CH_5^+.

We also calculated the dipole moment, which one obtains essentially for ''free'' in standard electronic structure codes, from the AIMD trajectories. Having an analytical form for the dipole surface, as well as the potential surface, enables us to calculate the vibrational spectrum of CH_5^+. For example, classically, the spectrum can be obtained from the Fourier transform of the dipole correlation function $\langle \boldsymbol{\mu}(t)\cdot\boldsymbol{\mu}(0)\rangle$. Such an analysis was described in Ref. 13. Here we will focus on the classical dipole correlation function. In particular, we discuss how this function provides information about the degree of delocalization of CH_5^+, even at energies that are well below the quantum zero-point energy.

Both the potential and dipole moment were fit to functional forms, as described next.

B. Fitting the potential and the dipole moment

The PES V is a function of the nuclear coordinates that is invariant under spatial translations, rotations, and reflections, and under the interchange of any pair of like nuclei. Since there are six $(N=6)$ nuclei, there are 12 $(3N-6)$ independent coordinates. However, we choose to use functions of all the 15 interparticle distances, i.e., redundant internal coordinates, to facilitate a fit that is fully symmetric with respect to permutation of any H atoms. The PES is of the form

$$V=p(x)+\sum_{i<j} q_{i,j}(x)y_{i,j}, \tag{2}$$

where x is a 15-dimensional vector with components $x_{i,j}=\ln(r_{i,j})$, $r_{i,j}$ is the distance between nuclei i and j, and $y_{i,j}$ is given by

$$y_{i,j}=\frac{e^{-r_{i,j}}}{r_{i,j}}. \tag{3}$$

The functions p and q are multinomials of all $x_{i,j}$ of order 7 and 3, respectively, and are constructed to satisfy the permutation symmetry with respect to the five hydrogen atoms. This symmetrization procedure is described in detail in the first section of Appendix A.

As described in detail in the following section most of the data is generated by AIMD calculations. While this approach ensures that the total energy is fixed at a desired value, the data set is highly correlated and so only a fraction of the data is ''useful'' for the fit. Thus, additional potential energies were obtained using grids in normal coordinates. These grids varied in mathematical dimensionality from 1 to 4 according to procedures adopted in the code MULTIMODE.[21]

Finally, the coefficients of the fit were computed by standard least squares fitting using singular value decomposition.[22] Both the potential energy and the gradients with respect to all six nuclear positions are used in the fit. Gradients have units of hartree/bohr, and in those units, the gradients were weighted by a factor of 0.1 relative to the potential energies, which are in hartrees. It was found empirically that a much larger weighting on the gradients hardly gives a more accurate gradient, but a much smaller weighting loses accuracy on the gradient while gaining at most a factor of 2 in the accuracy of the potential.

Unlike the potential energy, which is a scalar quantity, the dipole moment is a vector quantity. Therefore, it, or, more precisely, its vector components cannot be fit in terms of the internuclear distances. We choose to fit the dipole moment in a manner inspired by plasma kinetic theory,[23] in terms of reduced tensorial Hermite polynomials of the nuclear Cartesian coordinates. A detailed description of the model used to fit the dipole moment function is given in the second section of Appendix A.

C. Diffusion Monte Carlo calculations

The DMC studies follow the approach that was originally described by Anderson.[24,25] In this approach, the ground state wave function of CH_5^+ is represented by an ensemble of walkers; a set of δ functions, the positions of which are adjusted at each time step in the simulation according to the time-dependent Schrödinger equation, in which t is replaced by $-i\hbar\tau$. Our approach is described in detail elsewhere.[26,27] Briefly, the solution to the imaginary time, time-dependent Schrödinger equation is obtained through a random walk over a series of small time steps so that

$$\Psi(\tau)=e^{-\tau(\hat{H}-E_0)}\Psi(0)=\prod e^{-\Delta\tau(\hat{V}-W)}e^{-\Delta\tau\hat{T}}\Psi(0), \tag{4}$$

where $W=E_0$ and in the limit of infinite τ, $\Psi(\tau)$ becomes the ground state wave function. Operationally, $\Psi(\tau)$ is described by an ensemble of localized wave functions or walkers, each of which has equal weight. At each time step, the position of each walker is adjusted by a $3N$ dimensional vector δ. The value of each Cartesian component of δ is taken from a Gauss-random distribution with width in each of the eighteen Cartesian dimensions $\sigma_i=\sqrt{\Delta\tau/m_i}$ and m_i is the mass associated with the ith Cartesian coordinate.[24] This accounts for the kinetic part of the propagator. The integer part of the $e^{-(\hat{V}-W)\Delta\tau}$ term in the propagator indicates how many walkers will exist at that particular configuration, while the fractional part of this term gives the probability that an additional walker will be introduced at these coordinates. Finally,

$$W(\tau)=\overline{V}-\alpha\frac{N(\tau)-N(0)}{N(0)}, \tag{5}$$

where $\overline{V}$ represents the average value of the potential and $N(\tau)$ gives the number of walkers at time τ. This term ensures that the total number of walkers is roughly constant throughout the simulation. It also provides an approximation to the zero-point energy of the system.

The number of walkers, time step, and value of α were tested to ensure that the results were not sensitive to these choices. We use a time step of 1 a.u. with an ensemble containing 20 000 walkers at $t=0$ and $\alpha=0.01$ hartree. The system is allowed to equilibrate for 2000 time steps. Following that, the simulations are run for an additional 40 000 time steps. In order to ensure that the wave function has the correct permutation symmetry, at each time step the positions of a randomly chosen pair of hydrogen atoms were exchanged. This is found to have no effect on the calculated energies, within the reported statistical uncertainties. This can be understood through the observation that when all of the walkers are all placed at the same potential minimum, after 50 time steps 30% of the walkers have moved to other minima, and in the 40 000 time steps of the simulation the system has had more than enough time to fully delocalize among the 120 equivalent minima.

At any time in the simulation, the distribution of walkers provides a Monte Carlo sampling for the ground state wave function. In order to obtain probability densities, and from

these distance distribution functions and expectation values, the wave function was sampled after every 2000 time steps and the number of descendents of each walker after 500 additional time steps.[28,29] This provides the relative magnitude of $|\Psi|^2$ at the position of the walker.

Four types of results for the DMC simulations are reported. The first is the zero-point energy. This is obtained by calculating the average value of $W(\tau)$, from Eq. (5) for each of the simulations. The reported values and uncertainties for the zero-point energies are obtained by averaging these results over at least seven independent simulations. The second set of quantities we investigate is the average values and distributions in the HH and CH bond lengths. Due to the high symmetry and low barriers between the 120 minima on the CH_5^+ potential surface, all five CH bonds are, on average, equivalent, as are all ten HH bond lengths. As such, these results reflect the averages over all of these distances. Here the average values, widths, and distributions are obtained using the probably amplitudes obtained from the descendent weighting approach, described above.[28–30] In other words, these results reflect weighted averages over all of the walkers where the weight is determined by the number of descendents that walker has. The radial distribution functions are obtained by integrating the DMC probability amplitude over all coordinates except the coordinate of interest. Due to the symmetry of CH_5^+, the DMC distributions will be the same for each of the five r_{CH} or ten r_{HH}. Operationally, this is achieved by evaluating

$$P(r') = \int dV |\Psi|^2 \delta(r - r'), \tag{6}$$

where r represents either a CH or HH bond length.

The third quantity that is reported is projections of the probability amplitude along the coordinates that correspond to the two isomerization coordinates for this system. In the case of the lower energy saddle point, the motion across this transition state corresponds to a 60° rotation of the CH_3^+ group with respect to a torsional axis that connects the center of mass of the CH_3^+ subunit to the carbon atom. The higher energy transition state requires H-2 to flip between H-1 and H-3.

For each configuration of CH_5^+, obtained from the DMC simulation, the hydrogen atoms are numbered such that H-1 and H-2 form the closest pair. For rotation across the saddle point with C_s symmetry, the remaining three hydrogen atoms are numbered arbitrarily and we calculate the rotation of the CH-3 bond around the z axis that is defined to connect the carbon atom to the center of mass of the H_3 unit with the H-1; H-2 bond lying parallel to the xz plane. In the equilibrium, one of the three CH_3 hydrogen atoms will be in the xz plane and two will be rotated by approximately 60° out of that plane. For the flip transition, we define H-2 to be the hydrogen atom in the H-1; H-2 pair that is closest to one of the remaining three hydrogen atoms, which is then numbered H-3. The isomerization coordinate is the difference between the H-1; H-2 and the H-2; H-3 distances. As such, at the saddle point this quantity will be zero, while it is 0.43 Å at the equilibrium configuration. Projections of the DMC amplitude on these coordinates are obtained by binning the walkers according to the values of the isomerization coordinates and summing the probability amplitude in each bin.

The fourth and final quantity that is calculated from the DMC simulations is the vibrationally averaged rotational constants. Since these quantities are generally fit to experiment, there is no model-free operator that can be used to unambiguously calculate these quantities.[30–32] On the other hand, the average of the three constants will be independent of the model used to evaluate them. As such, we only report the average of the three rotational constants. These are calculated by generating the inverse moment of inertia tensor at each configuration, evaluating the average values of these quantities, as is described above and, finally, diagonalizing the resulting matrix. We performed this analysis using several choices for the embedding of the body-fixed axis system as well as in a space-fixed axis system. All of these gave numerically identical results.

III. RESULTS AND DISCUSSION

A. AIMD trajectories and potential and dipole fits

The first AIMD trajectory was run for a total energy of 3000 cm^{-1}, with the initial conditions and *ab initio* method described above. (This energy was chosen under the assumption that the CH_5^+ dynamics would be ergodic, or nearly so at this energy, especially give the random assignment of initial momenta.) The trajectory was run for 8194 time steps using a time step of 5 a.u., which gave a total propagation time of 991 fs. This number of time steps was both feasible in terms of computer time and sufficiently long to obtain an adequately well-resolved Fourier transform of the dipole correlation function. However, because the main goal in running this trajectory is to utilize the potential and gradient data for a global fit to the PES, we need to have some idea of how much of the 12-dimensional space has been spanned by a single trajectory. Two simple tests were used: (1) visual examination of the trajectory (a movie of the 3000 cm^{-1} trajectory is available at http://www.emory.edu/CHEMISTRY/faculty/bowman/) and (2) examination of the dipole correlation function. The animation shows highly fluxional motion, indicating near ergodic-like behavior, and as expected the dipole correlation function showed highly complex behavior (discussed in more detail below). Clearly, CH_5^+ is highly fluxional even for the relatively low energy considered here of 250 cm^{-1} per degree-of-freedom, and undergoes rapid isomerization. Therefore, the molecule is sampling a large number of distinctly different conformations in phase space.

A histogram of the potential energies sampled by this trajectory is given in Fig. 2. As seen, the data nearly span the entire possible range of potential energies (0–3000 cm^{-1}); however, the most probable value of the potential energy is roughly half the total energy. (Similar results hold for the trajectories run at 1000 and 8000 cm^{-1}.) Therefore, if data were obtained along a single AIMD trajectory, the energy range over which the fit would be applicable would be governed by the total energy of the trajectory. In order to sample energetically distinct regions of the PES, we have run six AIMD trajectories at different total energies, i.e., two trajec-

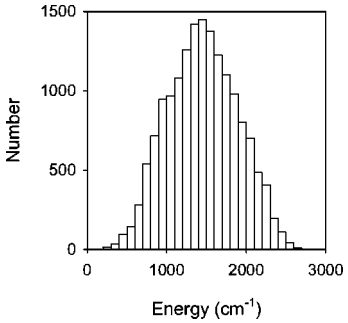

FIG. 2. Distributions of the potential energy sampled along a single AIMD trajectory with a total energy of 3000 cm^{-1}.

tories at 1000 cm^{-1} total energy (24 580 total time steps), three trajectories at 3000 cm^{-1} total energy (49 158 total time steps), and one trajectory at 8000 cm^{-1} total energy (8194 total time steps). The time step was 5 a.u. for the 1000 cm^{-1} trajectory and 10 a.u. for the 3000 and 8000 cm^{-1} trajectories. Doing trajectories at different total energies helps to overcome these limitations.

The first potential energy surface we reported[13] was based upon these AIMD trajectories and, thus, was only accurate to energies up to 8000 cm^{-1}. Since one goal of our overall work on CH_5^+ is to perform various quantum calculations, including the DMC calculations described here, it became clear that the surface had to be extended to regions of configuration space of much higher energy. This was done by adding 7619 *ab initio* energies generated on grids in normal coordinates, as described in Sec. II B. The reference geometry for these coordinates was taken as the C_{2v} saddle point.

Using the procedure outlined in Sec. II B a 2303-term fit was done to the data generated using these six trajectories plus the supplemental grid data. In order to conserve energy along the trajectories, the associated time steps (5 or 10 a.u.) are small. When the time step is small, the potential and gradient data generated at adjacent time steps is highly correlated and, therefore, data from every time step were not used in the fit but rather a subset of the data. For this fit, potential and gradient data from every tenth time step were used from each trajectory. The testing is done against all of the points and the rms fitting error for the potential energy is 51.0 cm^{-1} for the entire data set. For potential energies less than or equal to 20 000 cm^{-1}, the rms fitting error is 17.9 cm^{-1}. As with the initial 3000 cm^{-1} trajectory, CH_5^+ undergoes complicated dynamical motions both at the higher and the lower energies. A corresponding dipole moment fit was performed using the procedure outlined in Sec. II C. The fit reproduces the *ab initio* dipole values to within a few percent at worst.

B. Tests of the fitted PES

While the rms error indicates that the fit is precise, the rms error only tests against the data that has been calculated along the AIMD trajectories or determined on the grid. In this section, we consider other aspects of the surface that were not explicitly included in the fit. Specifically, we test the accuracy of the fit in predicting several stationary points and associated normal mode frequencies. Also, several simple ''cuts'' will be taken through the potential and compared with new *ab initio* data, i.e., data not explicitly included in the fit. In this manner, we hope to characterize the accuracy of the fit in the energy ranges spanned by the trajectories and grids, and the possible extrapolation outside these energy ranges.

TABLE I. Comparison of harmonic vibrational frequencies (cm^{-1}) of CH_5^+, at the global minimum C_s(I) geometry, at the C_s(II) transition state geometry, and at the C_{2v} transition state geometry, from *ab initio* calculations and as determined from the PES.

	C_s(I)		C_s(II)		C_{2v}	
Mode[a]	*Ab initio*[b]	PES[c]	*Ab initio*[b]	PES[c]	*Ab initio*[b]	PES[c]
1	3273	3274	3279	3282	3284	3282
2	3171	3167	3134	3128	3168	3162
3	3035	3028	3077	3070	2910	2903
4	2719	2713	2737	2731	2747	2737
5	2523	2519	2499	2497	2682	2675
6	1581	1577	1611	1607	1476	1477
7	1499	1498	1502	1504	1456	1456
8	1474	1476	1479	1477	1411	1405
9	1301	1314	1337	1340	1320	1340
10	1289	1289	1146	1156	1252	1253
11	749	749	944	941	471	470
12	245	238	216i	218i	584i	592i

[a]The normal modes are numbered in order of decreasing frequency.
[b]Calculated at the cc-pVTZ/MP2 basis set/level of electronic structure theory.
[c]Calculated from the PES, described in the text.

We determined the geometries, energies, and normal modes of the three lowest lying stationary points using MP2 with the cc-pVTZ basis set. The structures of these stationary points are given in Fig. 1. These stationary points were also found on the fitted PES and the atom-atom distances agree with the *ab initio* values to within 0.001 Å. The PES and the *ab initio* energies at the C_s(II) saddle point are 43 and 42 cm^{-1}, respectively, and at the C_{2v} saddle point 193 and 190 cm^{-1}, respectively. The normal frequencies at the stationary points are given in Table I, where excellent agreement is seen.

In order to examine the accuracy of the fit at higher energies, we have considered several ''cuts'' through the PES. The energies computed along these cuts are compared with newly computed *ab initio* values that were not explicitly included in the fit. The first cut we considered is a rigid rotation of the H_2 moiety at the global minimum around the bisector axis of the HCH bond angle θ, with the other degrees of freedom fixed at the minimum values. Figure 3(a) shows the potential energy, relative to the global minimum energy, computed on the PES and from new *ab initio* calculations as the H_2 is rotated. As seen the maximum occurs at 90° and the PES energies are very close to the *ab initio* ones; the relative error does not exceed 20 cm^{-1}. If we let the CH_3^+ bond angles relax, keeping all bond lengths fixed, the energy at θ=90° is reduced to approximately 200 cm^{-1} above the global C_s(I) minimum.

The second cut that we have considered involves the distance between the H_2 center of mass and the carbon atom,

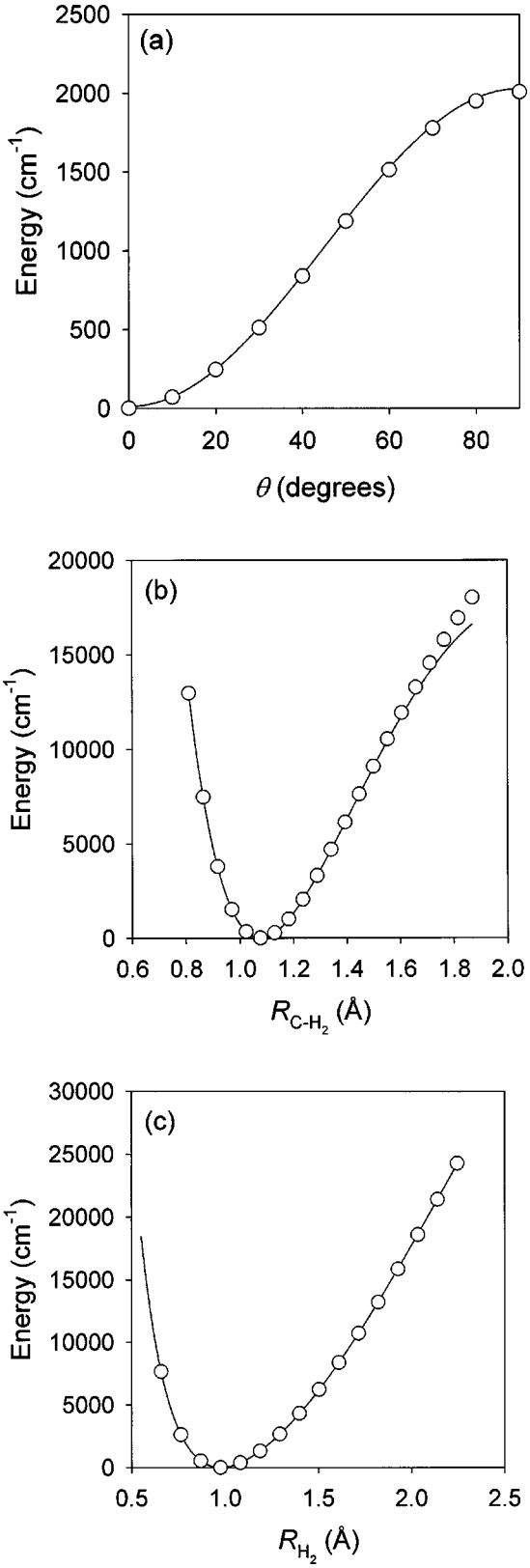

FIG. 3. Plot of the potential energy as a function of (a) the rotation of the H_2 fragment by an angle θ about the $R_{C\text{-}H_2}$ axis, (b) the distance $R_{C\text{-}H_2}$ between the center-of-mass of the H_2 fragment and the carbon atom, and (c) the internal stretching distance of H_2. In all cases the PES fit is plotted with a solid line and independent *ab initio* data, which were not included in the original fit, are plotted with (O).

starting at the C_s(I) global minimum. Here, H_2 is moved along the axis that bisects the HCH bond angle, with all of the other degrees of freedom fixed at their equilibrium values. Figure 3(b) shows the comparison of the PES and newly computed *ab initio* energies as a function of this $R_{C\text{-}H_2}$ separation coordinate. Below 13 000 cm^{-1}, the potential energies on the fit and the *ab initio* ones are indistinguishable on the scale of the figure and the relative error between the fits and the *ab initio* results does not exceed 300 cm^{-1} in this region ($1.5 < R_{C\text{-}H_2} < 3.25$). Not surprisingly, the energies on the fit begin to deviate from the *ab initio* ones for energies greater than 13 000 cm^{-1} since limited data at these energies have been incorporated into the fits. However, even up to 15 000 cm^{-1}, the extrapolation is quite reasonable.

The final cut involves the H_2 bond length R_{H_2}, with all other geometrical parameters fixed at their values at the C_s(I) global minimum. The comparison between the PES and newly calculated *ab initio* energies is shown in Fig. 3(c). The PES reproduces the new *ab initio* data with energies up to 25 000 cm^{-1} to within 50 cm^{-1}; this maximum energy is far above any of the data used in obtaining the fit.

The tests of the fit based on the comparisons with new *ab initio* data, including normal mode analyses at three stationary points and to potential comparisons of three cuts through the full 12-dimensional PES, indicate that the interpolation and to a lesser extent the extrapolation accuracy of the fit appear to be excellent. Additionally, more global tests of the fits come from running dynamics on the fit. We have run numerous classical trajectories on the fit at a variety of total energies; these calculations as well as DMC calculations indicate that the PES does not contain any "pitfalls," i.e., the trajectories do not exhibit any strange discontinuities or divergences and the DMC walkers do not fall into any holes on the surface. In the following section, the results for two (low-energy) trajectories are briefly discussed.

C. Low-energy classical dynamics

One obvious advantage of a fit versus a strictly direct-dynamics approach is the ability to run many trajectories and/or to run each trajectory for essentially arbitrarily long times. Using the fit potential and the corresponding fit dipole moment function, we have obtained the dipole correlation functions, described above, at two different total energies: 100 and 1000 cm^{-1}. The trajectories were initiated at the C_s(I) global minimum and the initial momenta were obtained as discussed in Sec. II A. The trajectories were integrated for 900 000 time steps of 5 a.u. (total time of approximately 105 ps). (To obtain these plots from AIMD trajectories of the same length, would require 147 h, assuming 1 s per *ab initio* calculation of potential and gradient or 1 year, assuming 1 min per *ab initio* calculation of potential and gradient.)

The dipole correlation functions are shown in Fig. 4. At the lower energy, the value of the dipole correlation function oscillates slightly about the value 0.525 a.u. which is approximately the value at $t=0.0$. The picture becomes more complicated even at 1000 cm^{-1}. At this energy the system samples the fully available range from -0.525 to $+0.525$ a.u., while, over time scales of 1–5 ps, the range of the

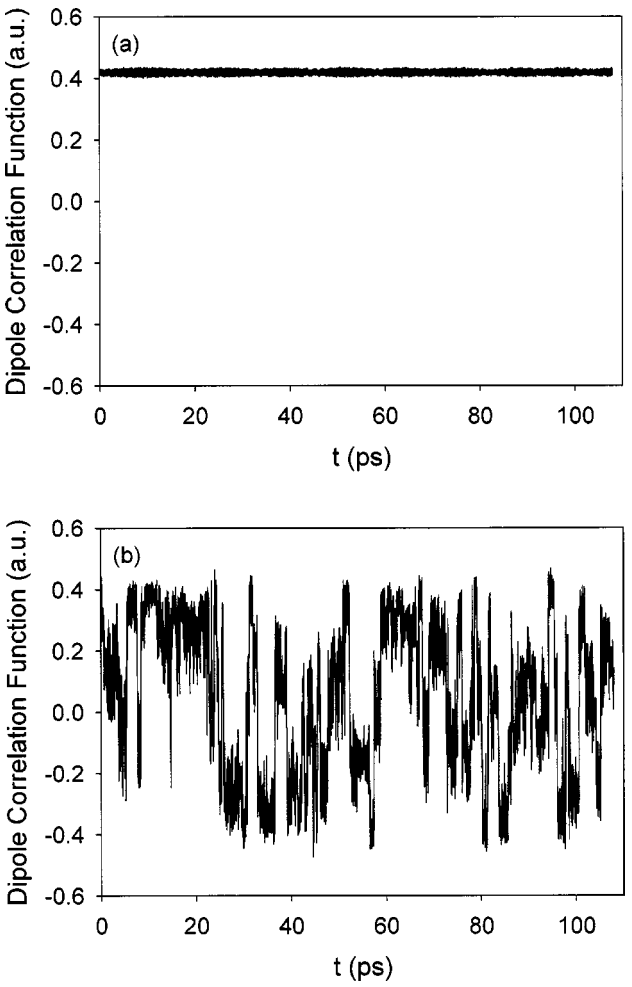

FIG. 4. Classical dipole correlation function for a single trajectory on the fit with total energies of (a) 100 cm^{-1} and (b) 1000 cm^{-1}.

fluctuations are much narrower, usually on the order of 0.20 a.u.. Since the trajectories are run at zero total angular momentum, the reorientation of the dipole moment reflects the fact that in all but the lowest energy simulation CH_5^+ is sampling multiple minima on the potential energy surface. The fact that the value of the dipole moment remains nearly constant over shorter times, even for the 1000 cm^{-1} trajectory, is an indication that the ion remains trapped in one or a small subset of minima over these time scales. Other measures of the localization of the dynamics, for example, the time evolution of the HH distances, further confirm these conclusions. These results are also in qualitative agreement with the previous Car-Parinello dynamics studies,[3,10–12] which determined the floppy nature of the CH_5^+ species. However, with potential energy surface and dipole moment fits, we can examine the dynamics in depth classically and, we can study them using more rigorous semiclassical and quantum mechanical methods; as done in the following sections, where we discuss and compare DMC calculations to classical results.

D. DMC results

The information that is immediately accessible by DMC is the zero-point energy of the system. As the classical dynamics, discussed above, indicates, even at 1000 cm^{-1} a classical description of this cation shows that it samples all of the available isomers over relatively short times. This energy is small compared to the harmonic zero-point energy of 11 421 cm^{-1}, calculated from the frequencies reported in Table I. Deuteration lowers this value to 8334 cm^{-1}, but still this is well above the 1000 cm^{-1} at which the classical trajectories were run. Based on the fact that the classical system is able to sample all 120 equivalent minima it is anticipated that the system will be highly anharmonic and delocalized, even in its vibrational ground state. This is borne out in the zero-point energy, calculated using DMC. For CH_5^+, the anharmonic zero-point energy is 10 975(5) cm^{-1} or 4% below the harmonic value. For CD_5^+, the zero-point energy is lowered by 3% to 8080(5) cm^{-1}. In both cases, the number in parentheses represents the uncertainty in the DMC energy. In the case of CH_5^+, recent semiclassical calculations of the zero-point energy by Kaledin *et al.*[33] yield a value of 10 973 cm^{-1}, using the same surface, which is in excellent agreement with the value obtained by DMC.

While the zero-point energy provides an indication into the degree of delocalization and anharmonicity of CH_5^+, these effects can be seen even more clearly through an analysis of the distributions of the CH and HH distances. In the C_s(I) stationary point configuration, the five CH distances and ten HH distances have the values, plotted with vertical lines in Fig. 5. Since, in a harmonic oscillator (HO) treatment, the potential is expanded about one of the 120 equivalent minima, the five hydrogen atoms are distinguishable. In contrast, for the zero-point quantum level or a classical trajectory run at that energy, the system samples all 120 minima and all of the hydrogen atoms are, on average, equivalent. As such, we focus this discussion on the overall CH and HH distance distributions, where these can be thought of as the average of the five or ten distributions from the harmonic analysis or the distribution for one of the CH or HH distances obtained from the DMC or molecular dynamics (MD) simulations. These are plotted in Fig. 5, while the average value and widths of the distributions are reported in Table II.

In the case of the CH distance distribution, taking just the equilibrium values, the average value is 1.13 Å and the standard deviation is 0.05 Å. As such, roughly half of the width reflects the range of CH distances in the cation, while the rest reflects the zero point amplitude of the CH stretch vibrations. The DMC and harmonic distributions are very similar, while the classical one is shifted to shorter distances and is slightly narrowed. The similarity between the harmonic and DMC distributions is consistent with the fact that the large amplitude motion required for CH_5^+ to sample the 120 potential minima reflects motions along coordinates that are orthogonal to the CH stretches. The shift between the MD and quantum distributions reflects the ability of the wave function to sample regions of the potential that are inaccessible in the classical description.

The HH distributions show a similar story. Taking only the distribution of the equilibrium values of the ten HH distances, the average value is 1.712 Å while the width of the distribution is 0.308 Å. In this case, this factor alone accounts for the widths of the distributions reported in Table II.

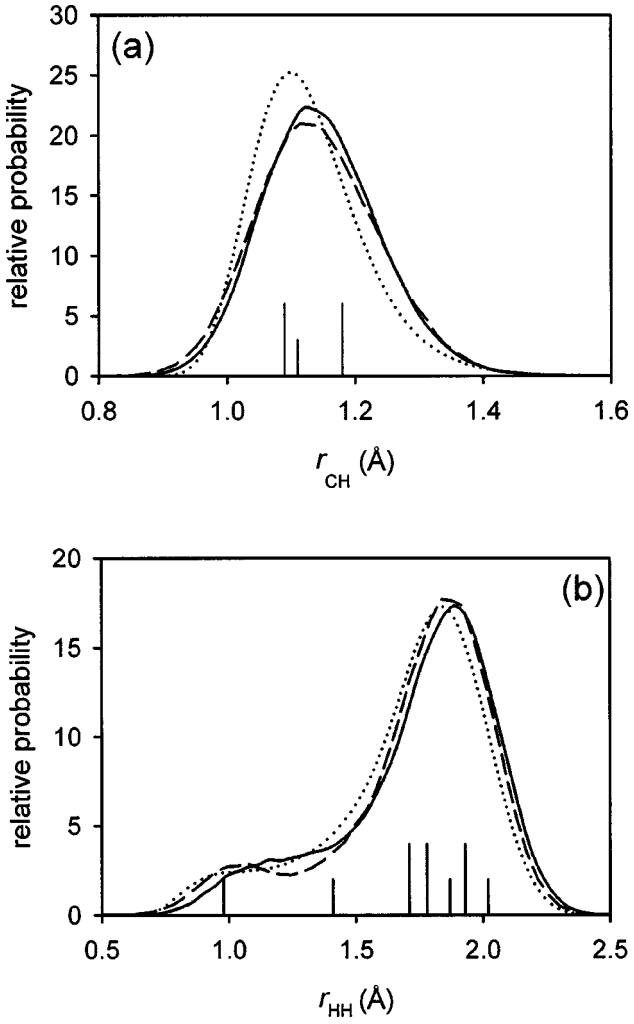

FIG. 5. Projections of the DMC (solid line), HO (dashed line), and MD (dotted line) distributions onto (a) the CH distance and (b) HH distance coordinates. In both plots, the vertical lines provide the values of these distances at the minimum energy configuration, while the length of these lines provides a measure of the number of distances that have that value.

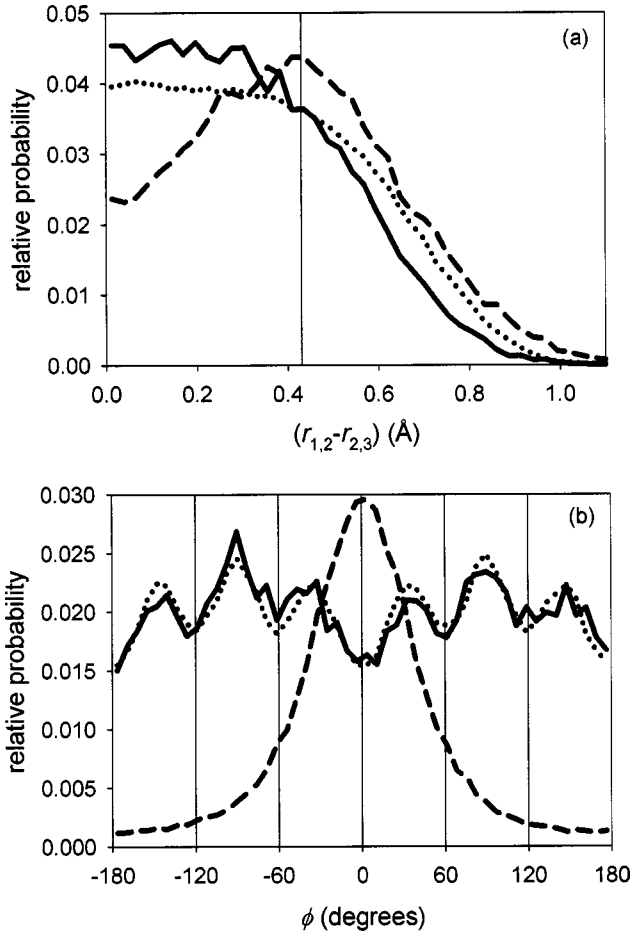

FIG. 6. Projections of the probability distributions onto (a) the flip isomerization and (b) the rotation isomerization coordinates, described in the text. In all cases, the thick solid line provides the results of the DMC ground state, the dashed line is obtained from the harmonic ground state, while the dotted distribution is obtained from the MD simulation. The equilibrium value of the coordinates are shown with thin vertical lines. The saddle points are located at $r_{1,2}-r_{2,3}=0$ in (a) and half way between the minimum energy values in (b).

Comparing the quantum and classical distributions shows a shoulder stretching from 0.7 to 1.3 Å and a larger peak centered at 1.8 Å. These distributions are consistent with the picture that was obtained from the lower energy classical trajectories, one of the HH distances is, on average, much smaller than the remaining nine ones.

TABLE II. Comparison of the zero-point energies, average CH and HH distances and widths obtained from DMC ground state calculations, the MD simulations at the DMC zero-point energy and a harmonic analysis.

Ion method	CH_5^+ DMC	CH_5^+ MD	CH_5^+ HO	CD_5^+ DMC	CD_5^+ MD	CD_5^+ HO
ZPE/cm^{-1} [a]	109 75 (5)		11421	8080 (5)		8334
$\langle r_{CH}\rangle$/Å	1.147	1.146	1.142	1.143	1.140	1.138
Width/Å [b]	0.091	0.085	0.095	0.082	0.074	0.084
$\langle r_{HH}\rangle$/Å	1.746	1.738	1.730	1.738	1.732	1.725
Width/Å [b]	0.309	0.309	0.315	0.306	0.304	0.309

[a]The number in parentheses, following the DMC result, represents one standard deviation, based on at least five independent simulations.
[b]The width provides the width of the distribution of HH or CH distances.

A third way to analyze the degree of localization of the wave function is to ask what fraction of the amplitude is located in each of the 120 equivalent minima. In the case of the DMC and MD results, the distribution has equal amplitude in each of the minima, whereas the harmonic ground state only has 75% of its amplitude in the minimum around which it is expanded and more than 99% of the amplitude is in either this minimum or the three minima that are connected to it through the C_{2v} and C_s(II) transition states.

The above results imply that the system is fairly well localized along some of the coordinates, but in order for the quantum mechanical ground state to sample all 120 minima it must be delocalized along others. To further characterize and compare this delocalization, we project the DMC, HO, and MD distributions onto the two coordinates that correspond the two low-energy isomerization pathways. These are plotted in Fig. 6. In the case of the *flip-isomerization* coordinate, which corresponds to transitions over the C_{2v} transition state, the equilibrium geometry corresponds to a value of 0.42 Å. Since the harmonic description is based on an expansion about one of the minima, this distribution is maxi-

mized at the equilibrium configuration, but contains substantial amplitude at the C_{2v} saddle point. In contrast the MD and DMC distributions are flat between the transition state and the equilibrium configuration. The second isomerization coordinate corresponds to sixfold rotation of the CH_3^+ and H_2 subgroups. The minimum energy configurations correspond to angles of 0°, ±60°, ±120°, and 180°, while the intermediate angles correspond to the C_s(II) transition state. The harmonic distribution is peaked at 0°, while the classical and DMC distributions each have six peaks. Interestingly these peaks are located at the C_s(II) saddle points rather than at the C_s(I) minimum energy configuration.

Clearly there are differences between the localized HO description and the delocalized MD and DMC descriptions. One major difference, based on the transition state projections presented above, is that in both the DMC and MD descriptions the system is more likely to be found in configurations near the transition states than the minimum energy geometries, as necessarily predicted by the HO description. To understand these unusual features, we turn to the harmonic analysis at the various stationary points. When we add the corresponding zero-point energies to the energies at the three stationary points reported in Table I, we find that the C_s(II) saddle point is 10.6 cm^{-1} *below* the C_s(I) minimum and the C_{2v} saddle point is 150.6 cm^{-1} *below* the C_s(I) minimum. Although these numbers will shift when anharmonicity is included, the picture is consistent with the plots in Fig. 6. To further verify this trend, we calculated the distributions and energies for CD_5^+ and CT_5^+ as a function of ϕ. For these isotopomers, the C_s(II) saddle point is 3.4 and 10.2 cm^{-1}, respectively, *above* the C_s(I) minimum when harmonic zero-point energies are taken into account. The corresponding distributions are plotted in Fig. 7. Increasing the mass of hydrogen has virtually no effect on the MD distributions, as expected, since zero-point effects are absent in MD simulations. By contrast the peaks in the DMC distributions shift from being at the position of the C_s(II) saddle point, for CH_5^+, to at the position of the C_s(I) saddle points for CT_5^+, as expected based on zero-point arguments.

Finally, we consider the vibrationally averaged rotational constants. As stated above, there is no unambiguous definition of these quantities in terms of expectation values of operators since they are parameters in an effective Hamiltonian to which experimental rotation-vibration transitions are fit. If we consider the equilibrium structure of the ion, the three rotational constants are distinct, as seen in Table III, and the range of the values is roughly 20% of the average rotational constant. This reflects the C_s symmetry of the equilibrium configuration. On the other hand, the system undergoes large amplitude vibrational motions, even in its vibrational ground state. Given the very large amplitude motion along the isomerization coordinates, displayed in the plots in Fig. 6, we anticipate that the molecule will be a spherical top, although the vibrational angular momentum resulting from, in particular, the large amplitude motion along the sixfold torsional potential may lead to effective constants that appear distinct. As such, we only report the average of the three rotational constants, obtained for CH_5^+ and its isotopically substituted analogs. It is interesting to note that when we perform the above analysis on the classical distribution of configurations, obtained by running the trajectory at the zero-point energy of the system, we obtain averaged rotational constants that are nearly identical to the reported DMC values. As these values will be sensitive to the energy at which the trajectory is run, while the classical and DMC results are similar for the same energy, knowing the energy at which the MD needs to be run requires a quantum mechanical treatment.

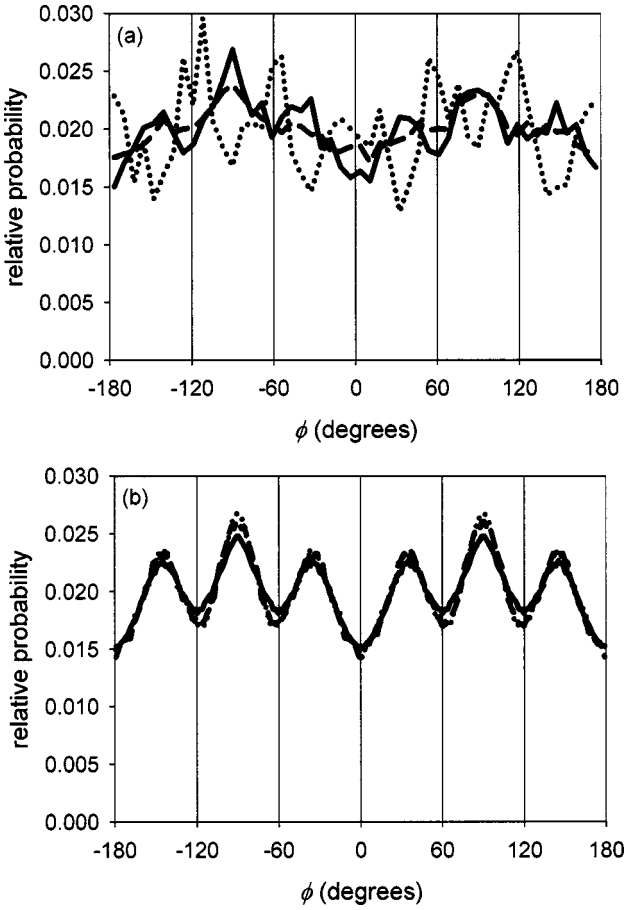

FIG. 7. Projections of the probability distributions onto the rotation isomerization coordinate for CH_5^+ (solid line), CD_5^+ (dashed line), and CT_5^+ (dotted line), obtained from the (a) DMC and (b) MD distributions, as described in the text.

IV. SUMMARY AND CONCLUSIONS

In this paper we presented a procedure to use *ab initio* potential and gradient data generated from direct dynamics

TABLE III. Comparison of the rotational constants (in cm^{-1}), calculated from the lowest energy structure of CH_5^+ and those obtained by averaging the constants over the ground state wave function and classical distributions, described in the text.

Ion	A_e	B_e	C_e	EQ[a]	DMC[a]	MD[a]
CH_5^+	4.46	3.91	3.71	4.03	3.91	3.93
CD_5^+	2.23	1.97	1.87	2.02	1.98	2.00
CT_5^+	1.49	1.33	1.26	1.36	1.34	1.34

[a]Average of the three rotational constants, obtained from the equilibrium configuration (EQ), DMC, or MD calculations, as indicated.

calculations run at several energies to obtain a fitted potential energy surface. The dipole moment was also obtained and fit. A key aspect of the approach, which made it both feasible and highly accurate for the challenging fluxional ion CH_5^+, was that the polynomial basis used in the fit incorporates the full permutational symmetry of the system. The resulting PES was tested against the original *ab initio* data set and against new *ab initio* data calculated along selected ''cuts'' of the potential, and the agreement is excellent in both cases. We also learned that only a fraction of the data from direct dynamics need be used in fitting, because data from adjacent time steps is too similar to be effectively used in a fit. This suggests a strategy where a fit based on a low-level method is used to generate configurations for higher level *ab initio* calculations to be used in a final fit. We are investigating this in new applications of this approach.

The PES was used in DMC, classical MD, and standard HO calculations of the nuclear dynamics. The classical dipole correlation function was obtained at two energies. At very low energy the small amplitude oscillations of this function illustrated highly localized motion of CH_5^+ about a single minimum, while at a higher energy, the system clearly displayed highly fluxional motion over many minima. The DMC calculations focused on the zero-point energy and properties of CH_5^+ with some analysis also for CD_5^+ and CT_5^+. Comparisons were made with MD results run at the corresponding quantum zero-point energies. Both calculations find that CH_5^+ samples all 120 equivalent minima and yield very similar CH and HH distance distributions for CH_5^+. However, when we consider projections of the distributions along other coordinates, specifically those associated with the two types of motions that are needed to go across the C_s(II) or C_{2v} saddle points, differences in localization emerge between the rigorous DMC and approximate MD pictures. These differences were rationalized by a simple harmonic analysis of the effective barriers at the minimum and these saddle points demonstrating the importance of quantum effects for this system.

While the results of the classical and DMC studies provide insight into the dynamics and spectrum, there are of course limitations. For example, the present DMC calculations are limited to the structure and properties at the zero-point energy. An investigation of the vibrational structure and spectroscopy will require a method for calculating the quantum excited state energies and wave functions. The high dimensionality and highly fluxional behavior of CH_5^+ makes basis set calculations extremely challenging while DMC, being primarily a ground state method, is not particularly efficient for calculating many vibrationally excited states. Future studies will address this, albeit with some approximations. For example, we are applying the code MULTIMODE,[21] in both its conventional single reference and ''reaction path'' versions, to obtain the zero-point and excited states. We are also investigating several ''fixed-node'' DMC approaches to obtain excited states, and we are continuing to investigate the structure of mixed isotopomers of the CH_5^+ system for which we find that the system becomes much less delocalized.[15]

ACKNOWLEDGMENTS

The authors thank the National Science Foundation for support (Grant No. CHE-0200968) (A.B.M.), and (Grant Nos. CHE-0131482 and ITR CHE-0219331) (J.M.B.) A.B.M. also thanks the Dreyfus Foundation awards program for support. B.J.B. thanks Professor Gregor Kemper and Mr. Allan Steel for advice about invariant computations and Magma. We thank Dr. Stephan Irle for useful discussions on performing *ab initio* calculations and Xinchuan Huang for setting up the normal-coordinate grids for doing *ab initio* calculations.

APPENDIX A: POTENTIAL AND DIPOLE MOMENT SURFACES

1. Potential fit

In our earlier paper[13] we represented the potential as a polynomial in the inverse internuclear distances, $V=p(x)$, in which the 15-component vector x is given by $x_{i,j}=1/r_{i,j}$, where $r_{i,j}$ is the distance between nuclei i and j with indices i and j in $\{0,...,5\}$ and $i<j$. An index value of 0 denotes the carbon nucleus and index values of 1–5 refer to the hydrogen nuclei. Representing the potential as a function of internuclear distances immediately assures that it is invariant under the point group operations: translations, rotations, and reflections. Furthermore, the coefficients of the polynomial were constrained to obtain complete permutational symmetry among the five hydrogen nuclei.

That representation as a polynomial in the inverse distances was chosen because it allows the correct behavior, $V \rightarrow$ const. as some $r_{i,j}\rightarrow\infty$, but the fitted potential could not be very accurate in the higher energy regions where some distance $r_{i,j}$ becomes small. In the present work we are interested in higher energies than employed in Ref. 13, but still below the dissociation energy, and so we modified the form of the fit.

We now employ two kinds of terms. The first term is a polynomial $p(x)$, but now we use $x_{i,j}=\ln(r_{i,j})$ instead of the inverse distance. In addition there is a second set of terms of the form $q_{i,j}(x)y_{i,j}$; one such term for each i, j pair. Here, the $q_{i,j}$ are polynomials in x and the multiplying factor is $y_{i,j}=\exp(-r_{i,j})/r_{i,j}$; these additional terms are introduced to allow a representation of the strong repulsion at small $r_{i,j}$. So,

$$V=p(x)+\sum_{i<j} q_{i,j}(x)y_{i,j}. \tag{A1}$$

We have used a seventh degree polynomial for p and third degree polynomials for the $q_{i,j}$, again with coefficients restricted so that V is completely symmetric with respect to permutations among the H nuclei. Most of the algorithmic complexity is in specifying the approximation space for the polynomial p.

The problem of specifying a basis of the space of polynomials invariant under some permutation symmetry belongs to computational invariant theory and specifically the theory of invariants of finite groups. For our implementation we relied heavily on the exposition of computational invariant

theory by Derksen and Kemper[34] and we also made use of the procedures for invariant computation[35] in the Magma computer algebra system.[36]

For the present problem we require a basis, truncated at some degree, for polynomials of x that are invariant under the symmetric group Sym(5) acting on the 15-dimensional space of x by a certain permutation of the variables, which we now describe. Let $\sigma \in \mathrm{Sym}(5)$ and let it act on the index set {0,...,5} by permuting the five hydrogenic indices {1,...,5} and leaving the carbon index 0 unchanged. Then σ acts on the components of our 15-element vector x by σ: $x \to x'$, where $x_{k,l} = x_{i,j}$ for all index pairs (i,j); here $k = \min[\sigma(i),\sigma(j)]$ and $l = \max[\sigma(i),\sigma(j)]$. This is not the natural representation of Sym(5) and the basis has to be obtained computationally.

A Magma computation gives very quickly, by way of the Hilbert Series, the dimension of the relevant space of invariant polynomials at each degree: There is one independent invariant polynomial at degree 0, two independent invariant polynomials at degree 1, and then 7, 22, 69, 198, 550, and 1441 invariant polynomials, respectively, at degrees 2–7. The total dimension of the approximation space at polynomial degree up to 7 is therefore 2290.

At the time that we set up the polynomial fit for the present studies we were not able to obtain the complete basis of the space of invariant polynomials at degree 7—we had the basis up to degree 6, and at degree 7 we had only those basis polynomials that could be expressed as product of basis elements used at lower degree—and the results reported in this paper were obtained using a basis of size 2239 for the invariant polynomials up to degree 7 rather than the complete basis of size 2290. Meanwhile a new release of Magma (Version 2.10-19) containing improved algorithms for invariant computation makes it easy to compute the complete basis. The code for our latest CH_5^+ fitted potential is available from the authors.

2. Model for the dipole moment

The dipole moment is a vector quantity and so it cannot be represented as a function of just the (scalar) internuclear distances. Instead we represent the dipole moment in a manner inspired by plasma kinetic theory,[23] in terms of reduced tensorial Hermite polynomials of the nuclear coordinates. We only carried this through to low order, and describe it here only as it was applied to CH_5^+. In the present work all coordinates are in the center of mass frame and the dipole moment is defined with respect to the center of mass.

Let $\mathbf{r}(0)$ be the location of the carbon nucleus and $\mathbf{r}(1)$–$\mathbf{r}(5)$ the locations of the hydrogen nuclei. Let

$$\mathbf{u} = \frac{1}{5}\sum_{i=1}^{5} \mathbf{r}(i) \tag{A2}$$

and then

$$\mathbf{D} = \sum_{i=1}^{5} (\mathbf{r}(i)-\mathbf{u})(\mathbf{r}(i)-\mathbf{u})^T \tag{A3}$$

and

$$\mathbf{q} = \frac{1}{5}\sum_{i=1}^{5} \|\mathbf{r}(i)-\mathbf{u}\|^2(\mathbf{r}(i)-\mathbf{u}). \tag{A4}$$

$\mathbf{u}$ and $\mathbf{q}$ are vectors in $\mathbf{r}^3$ and $\mathbf{D}$ is a tensor or matrix. (In the language of kinetic theory, $\mathbf{u}$ would be a velocity, $\mathbf{D}$ a pressure tensor, and $\mathbf{q}$ a heat flux vector. We will not make further use of that analogy.) Let $d_0 = \mathrm{Trace}\,\mathbf{D}$ and let $\mathbf{E} = \mathbf{D} - d_0/3\,\mathbf{I}$, where $\mathbf{I}$ is the unit matrix. Finally let $s = 5\|\mathbf{u}\|^2 + d_0$. As basis functions for approximation of the dipole moment we take now the following five quantities, viewed as vector functions of the nuclear coordinates $\mathbf{r}(0)$,...,$\mathbf{r}(5)$:

$$\mathbf{f}_0 = \frac{\mathbf{u}}{s}, \tag{A5}$$

$$\mathbf{f}_1 = \frac{5\|\mathbf{u}\|^2\mathbf{u}}{s}, \tag{A6}$$

$$\mathbf{f}_2 = \frac{d_0\mathbf{u}}{s}, \tag{A7}$$

$$\mathbf{f}_3 = \frac{\mathbf{E}\cdot\mathbf{u}}{s}, \tag{A8}$$

and

$$\mathbf{f}_4 = \frac{\mathbf{q}}{s}. \tag{A9}$$

[1] P. R. Schreiner, S.-J. Kim, H. F. Schaeffer III, and P. von Ragué Schleyer, J. Chem. Phys. **99**, 3716 (1993).
[2] A. Kormornicki and D. A. Dixon, J. Chem. Phys. **86**, 5625 (1987).
[3] J. S. Tse, D. D. Klug, and K. Laasonen, Phys. Rev. Lett. **74**, 876 (1995).
[4] W. Klopper and W. Kutzelnigg, J. Phys. Chem. **94**, 5625 (1990).
[5] S. J. Collins and P. J. O'Malley, Chem. Phys. Lett. **228**, 246 (1994).
[6] M. Kolbuszewski and P. R. Bunker, J. Chem. Phys. **105**, 3649 (1996).
[7] H. Müller, W. Kutzelnigg, J. Noga, and W. Klopper, J. Chem. Phys. **106**, 1863 (1997).
[8] P. R. Schreiner, Agnew. Chem. Int. Ed. **39**, 3239 (2000).
[9] A. L. L. East, M. Kolbuszewski, and P. R. Bunker, J. Phys. Chem. A **101**, 6746 (1997).
[10] D. Marx and M. Parrinello, Z. Phys. D: At., Mol. Clusters **41**, 253 (1997).
[11] D. Marx and M. Parrinello, Nature (London) **375**, 216 (1995).
[12] D. Marx and M. Parrinello, Science **284**, 59 (1999).
[13] A. Brown, B. J. Braams, K. M. Christoffel, Z. Jin, and J. M. Bowman, J. Chem. Phys. **119**, 8790 (2003).
[14] E. T. White, J. Tiang, and T. Oka, Science **284**, 135 (1999).
[15] A. B. McCoy, B. J. Braams, A. Brown, X. Huang, Z. Jin, and J. M. Bowman, J. Phys. Chem. A **108**, 4991 (2004).
[16] L. Verlet, Phys. Rev. **159**, 98 (1967).
[17] C. Hampel, K. Peterson, and H.-J. Werner, Chem. Phys. Lett. **190**, 1 (1992).
[18] T. H. Dunning, Jr., J. Chem. Phys. **90**, 1007 (1989).
[19] A. El Azhary, G. Rauhut, P. Pulay, and H.-J. Werner, J. Chem. Phys. **108**, 5185 (1998).
[20] MOLPRO, a package of *ab initio* programs designed by H.-J. Werner and P. J. Knowles, version 2002.6, with contributions from R. D. Amos, A. Berhardsson, A. Berning *et al.*, Birmingham, UK, 2002.
[21] J. M. Bowman, S. Carter, and X.-C. Huang, Int. Rev. Phys. Chem. **22**, 533 (2003).
[22] E. Anderson, Z. Baj, C. Bischof *et al.*, LAPACK *Users' Guide*, 3rd ed. (SIAM, Philadelphia, 1999).
[23] R. Balescu, *Transport Processes in Plasma: Classical Transport Theory* (Elsevier, North Holland, 1988), Vol. 1.
[24] J. B. Anderson, J. Chem. Phys. **63**, 1499 (1975).
[25] J. B. Anderson, J. Chem. Phys. **65**, 4121 (1976).
[26] A. B. McCoy, Chem. Phys. Lett. **321**, 71 (2000).
[27] H.-S. Lee, J. M. Herbert, and A. B. McCoy, J. Chem. Phys. **110**, 5481 (1999).

[28] M. A. Suhm and R. O. Watts, Phys. Rep. **204**, 293 (1991).
[29] M. H. Kalos, J. Comput. Phys. **2**, 1967 (1967).
[30] P. Sandler, V. Buch, and J. Sadlej, J. Chem. Phys. **105**, 10387 (1996).
[31] A. Ernesti and J. M. Hutson, Chem. Phys. Lett. **222**, 257 (1994).
[32] H.-S. Lee and A. B. McCoy, J. Phys. Chem. **114**, 10278 (2001).
[33] A. L. Kaledin, S. D. Kunikeev, and H. S. Taylor, J. Phys. Chem. A **108**, 4995 (2004).
[34] H. Derksen and G. Kemper, *Computational Invariant Theory* (Springer, Berlin, 2002).
[35] G. Kemper and A. Steel, in *Computational Methods for Representations of Groups and Algebras*, Progress in Mathematics, Vol. 173, edited by P. Draexler, G. O. Michler, and C. M. Ringel (Birkhauser, Basel, 1999).
[36] W. Bosma, J. Cannon, and C. Playoust, J. Symb. Comput. **24**, 235 (1997).